

A HIGH FRACTION OF Ly α -EMITTERS AMONG GALAXIES WITH EXTREME EMISSION LINE RATIOS AT $Z \sim 2^*$

DAWN K. ERB¹, MAX PETTINI², CHARLES C. STEIDEL³, ALLISON L. STROM³,
GWEN C. RUDIE⁴, RYAN F. TRAINOR^{5,6}, ALICE E. SHAPLEY⁷, NAVEEN A. REDDY^{8,9}

DRAFT: May 5, 2022

ABSTRACT

Star-forming galaxies form a sequence in the [O III] $\lambda 5007$ /H β vs. [N II] $\lambda 6584$ /H α diagnostic diagram, with low metallicity, highly ionized galaxies falling in the upper left corner. Drawing from a large sample of UV-selected star-forming galaxies at $z \sim 2$ with rest-frame optical nebular emission line measurements from Keck-MOSFIRE, we select the extreme $\sim 5\%$ of the galaxies lying in this upper left corner, requiring $\log([\text{N II}]/\text{H}\alpha) \leq -1.1$ and $\log([\text{O III}]/\text{H}\beta) \geq 0.75$. These cuts identify galaxies with $12 + \log(\text{O}/\text{H}) \lesssim 8.0$, when oxygen abundances are measured via the O3N2 diagnostic. We study the Ly α properties of the resulting sample of 14 galaxies. The mean (median) rest-frame Ly α equivalent width is 39 (36) Å, and 11 of the 14 objects (79%) are Ly α -emitters (LAEs) with $W_{\text{Ly}\alpha} > 20$ Å. We compare the equivalent width distribution of a sample of 522 UV-selected galaxies at $2.0 < z < 2.6$ identified without regard to their optical line ratios; this sample has mean (median) Ly α equivalent width -1 (-4) Å, and only 9% of these galaxies qualify as LAEs. The extreme galaxies typically have lower attenuation at Ly α than those in the comparison sample, and have $\sim 50\%$ lower median oxygen abundances. Both factors are likely to facilitate the escape of Ly α : in less dusty galaxies Ly α photons are less likely to be absorbed during multiple scatterings, while the harder ionizing spectrum and higher ionization parameter associated with strong, low metallicity star formation may reduce the covering fraction or column density of neutral hydrogen, further easing Ly α escape. The use of nebular emission line ratios may prove useful in the identification of galaxies with low opacity to Ly α photons across a range of redshifts.

Subject headings: galaxies: evolution—galaxies: formation—galaxies: high-redshift

1. INTRODUCTION

Low metallicity galaxies may be the primary source of the radiation that reionized the universe. It is likely that many faint and probably low metallicity galaxies were required to supply a sufficient number of photons (Kuhlen & Faucher-Giguère 2012; Robertson et al. 2013, 2015), and ionizing radiation has been detected from galaxies with rest-frame optical line ratios indicative of low metal-

licity and high ionization parameter (Izotov et al. 2016; Vanzella et al. 2016). Until the launch of the *James Webb Space Telescope (JWST)* enables studies of galaxies in the reionization era, the most effective way to analyze low metallicity sources is through the detailed examination of galaxies at $z \lesssim 3$, when most of the strong rest-frame optical emission lines can be observed from the ground.

As the strongest feature in the ultraviolet (UV) spectra of many galaxies, the Ly α emission line is of particular interest: its strength depends on a galaxy's dust content and on the kinematics, column density, geometry and covering fraction of neutral hydrogen, all quantities that are also likely to influence the escape of Lyman continuum radiation (see Dijkstra 2014 for a recent review). However, the relative importance of these properties in setting the strength of Ly α emission is still uncertain.

Low metallicity galaxies at $z \sim 2$ that have been studied in detail typically have very strong Ly α emission (rest-frame Ly α equivalent width $W_{\text{Ly}\alpha} \gtrsim 50$ Å; Erb et al. 2010; Stark et al. 2014), but galaxies with high Ly α equivalent widths span a wide range in mass and can be old or dusty (e.g. Kornei et al. 2010; Hagen et al. 2014). Most Ly α -emitters (LAEs, defined as having $W_{\text{Ly}\alpha} > 20$ Å and usually selected via their Ly α emission) are fainter and lower in mass than galaxies selected via broad-band continuum colors (Gawiser et al. 2006; Guaita et al. 2011; McLinden et al. 2014), and these mass and luminosity differences between samples complicate efforts to determine the primary factors influencing Ly α emission. A useful technique is therefore the comparison of matched

* Based on data obtained at the W. M. Keck Observatory, which is operated as a scientific partnership among the California Institute of Technology, the University of California, and the National Aeronautics and Space Administration, and was made possible by the generous financial support of the W. M. Keck Foundation.

¹ Center for Gravitation, Cosmology and Astrophysics, Department of Physics, University of Wisconsin Milwaukee, 3135 N. Maryland Avenue, Milwaukee, WI 53211, USA; erb@uwm.edu

² Institute of Astronomy, Madingley Road, Cambridge CB3 0HA, UK

³ Cahill Center for Astrophysics, California Institute of Technology, 1216 E. California Blvd., MS 249-17, Pasadena, CA 91125, USA

⁴ Carnegie Observatories, 813 Santa Barbara Street, Pasadena, CA 91101, USA

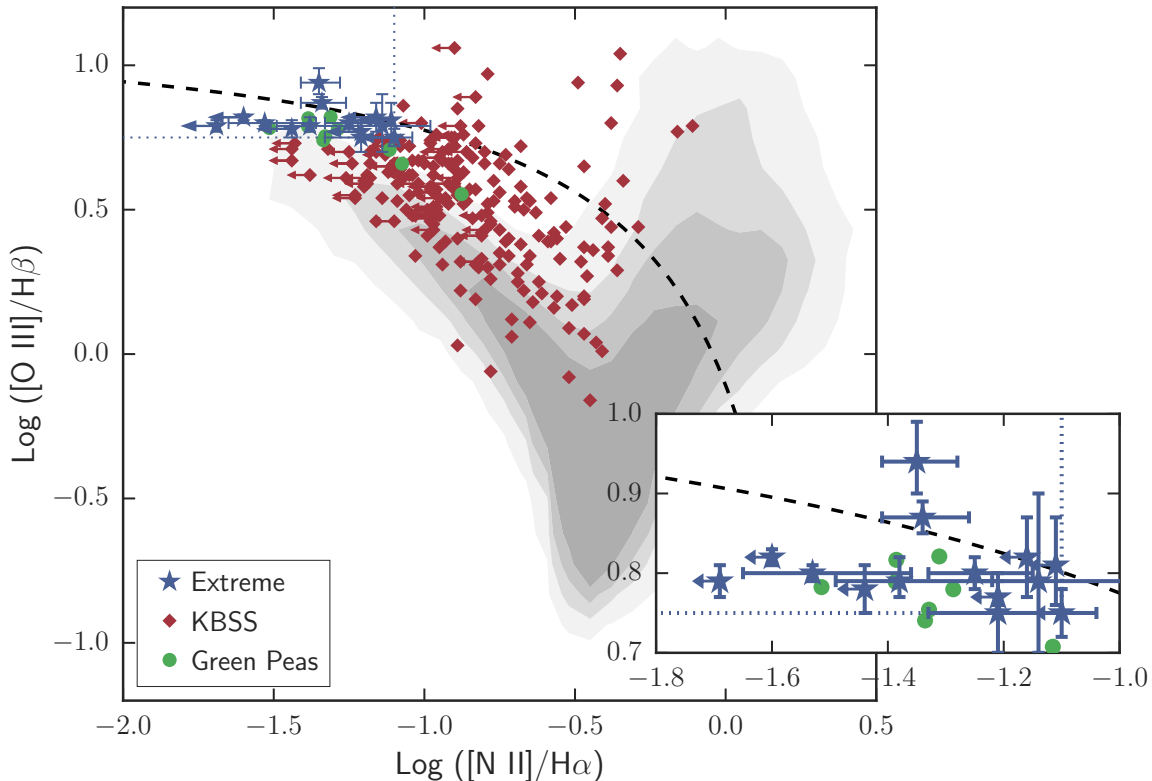
⁵ Department of Astronomy, University of California, Berkeley, 501 Campbell Hall, Berkeley, CA 94720, USA

⁶ Miller Fellow

⁷ University of California, Los Angeles, Department of Physics and Astronomy, 430 Portola Plaza, Los Angeles, CA 90095, USA

⁸ Department of Physics and Astronomy, University of California, Riverside, 900 University Avenue, Riverside, CA 92521, USA

⁹ Alfred P. Sloan Fellow



4959

FIG. 1.— The $[\text{O III}]/\text{H}\beta$ vs. $[\text{N II}]/\text{H}\alpha$ diagnostic diagram, in which star-forming galaxies fall on the left side and AGN in the upper right. The 14 galaxies in the extreme sample (blue stars) lie in the upper left corner, with $\log ([\text{N II}]/\text{H}\alpha) \leq -1.1$ and $\log ([\text{O III}]/\text{H}\beta) \geq 0.75$ (dotted blue lines). We also show the KBSS parent sample of Steidel et al. (2014) with red diamonds and Green Pea galaxies from Henry et al. (2015) with green circles. Grey contours show local galaxies from the Sloan Digital Sky Survey, and the black dashed line shows the maximum starburst line of Kewley et al. (2001). The inset panel shows a closeup view of the extreme region for clarity.

(in stellar mass or continuum magnitude) galaxy samples with and without $\text{Ly}\alpha$ emission; using this method, Kornei et al. (2010) found that $\text{Ly}\alpha$ -emitting galaxies at $z \sim 3$ are less dusty but older than comparable galaxies without $\text{Ly}\alpha$ emission, while Hagen et al. (2016) recently found no statistically significant differences between $\text{Ly}\alpha$ -selected and $[\text{O III}]$ -selected galaxies of the same masses at $z \sim 2$.

Because high redshift LAEs are faint, few have measurements of metallicity, ionization parameter, or other properties relying on the detection of weak nebular emission lines. Those measured tend to be at the bright end of the distribution, and generally have low metallicities, high ionization parameters, and little dust (Nakajima et al. 2013; Song et al. 2014). This appears to be true in the local universe as well: low metallicity galaxies with high equivalent width optical emission lines (the “Green Peas,” Izotov et al. 2011) have strong $\text{Ly}\alpha$ emission (Henry et al. 2015), while Cowie et al. (2011) find that LAEs have lower metallicities, bluer colors, and higher $\text{H}\alpha$ equivalent widths than galaxies with similar UV continuum magnitudes but without $\text{Ly}\alpha$ emission.

In this paper we examine the $\text{Ly}\alpha$ properties of a sample of galaxies at $z \sim 2$ selected to have extreme ratios of rest-frame optical emission lines. We identify galaxies lying in the upper left corner of the $[\text{O III}]\lambda 5007/\text{H}\beta$ vs. $[\text{N II}]\lambda 6584/\text{H}\alpha$ diagnostic diagram (the “BPT” diagram, Baldwin et al. 1981), which represents the low metallicity, high ionization end of the star-forming sequence. We then use the remainder of the parent sample

as a comparison sample for the extreme objects; relative to the extreme sample, this comparison sample has less extreme line ratios but approximately similar masses and continuum magnitudes.

We describe our data and sample selection in Section 2. In Section 3 we discuss the rest-frame optical emission line properties of the galaxies in the sample, and we quantify their $\text{Ly}\alpha$ emission in Section 4. We summarize and discuss our results in Section 5. We assume a Chabrier (2003) initial mass function and a cosmology with $H_0 = 70 \text{ km s}^{-1} \text{ Mpc}^{-1}$, $\Omega_m = 0.3$, and $\Omega_\Lambda = 0.7$ throughout.

2. DATA AND SAMPLE SELECTION

The galaxies discussed in this paper are drawn from the Keck Baryonic Structure Survey (KBSS; Steidel et al. 2004, 2014), for which objects are initially selected via rest-frame UV color criteria designed to identify star-forming galaxies at redshifts $2 \lesssim z \lesssim 2.6$. The parent sample for this work consists of 315 galaxies in the redshift range $1.95 \lesssim z \lesssim 2.65$ for which measurements (or upper limits in the case of $[\text{N II}]\lambda 6584$) of $\text{H}\alpha$, $[\text{N II}]\lambda 6584$, $[\text{O III}]\lambda 5007$ and $\text{H}\beta$ have been obtained with the Multi-Object Spectrometer for InfraRed Exploration (MOSFIRE; McLean et al. 2010, 2012) on the Keck I telescope. An earlier version of this parent sample, with 219 galaxies, was described in detail by Steidel et al. (2014), and we refer the reader to that paper for details of the MOSFIRE observations and data reduction.

For this work, we select the extreme $\sim 5\%$ of the KBSS sample based on position in the $[\text{O III}]/\text{H}\beta$ vs. $[\text{N II}]/\text{H}\alpha$

(BPT) diagnostic diagram. Low metallicity, highly ionized galaxies lie in the upper left corner, and the most extreme $\sim 5\%$ have both $\log([\text{N II}]/\text{H}\alpha) \leq -1.1$ and $\log([\text{O III}]/\text{H}\beta) \geq 0.75$ (see Figure 1). These thresholds are motivated by the general position of the extreme galaxy Q2343-BX418 (Erb et al. 2010) in the BPT diagram, as we wish to identify similar objects.

Fourteen galaxies with redshifts $2.17 < z < 2.47$ and mean (median) redshift $z = 2.30$ (2.30) fall in this region of the diagram, including seven objects with 3σ upper limits on $[\text{N II}]$ emission such that $\log([\text{N II}]/\text{H}\alpha) \leq -1.1$. We refer to these 14 galaxies as the extreme sample, and the galaxies and their rest-frame optical emission line properties are listed in Table 1.

Most of the rest-frame UV spectroscopic observations of the 14 extreme galaxies were obtained prior to the MOSFIRE observations, using the the Low Resolution Imaging Spectrometer (LRIS, Oke et al. 1995; Steidel et al. 2004) on the Keck I telescope. LRIS observations and data reduction are described by Steidel et al. (2004). Eight of the 14 galaxies (Q0100-BX239, Q0142-BX165, Q0207-BX74, Q0207-BX87, Q0207-BX144, Q0821-BX102, Q0821-BX221, and Q1700-BX711) were observed with the LRIS-B 400-line grism, offering spectral resolution of $\sim 500 \text{ km s}^{-1}$, while the remaining 6 (Q1217-BX164, Q1700-BX553, Q2206-BM64, Q2343-BX418, Q2343-BX460, and Q2343-BX660) were observed with the 600-line grism, providing $\sim 300 \text{ km s}^{-1}$ resolution. Most of the objects were observed with the standard KBSS integration time of 3×1800 seconds, but Q1700-BX553, Q2343-BX418, Q2343-BX460, and Q2343-BX660 were placed on masks that received between 5 and 11 hours of integration. Because of the varying integration times, the rest-frame UV spectra of the extreme subsample vary widely in S/N; for this reason, we focus here on the Ly α properties of the galaxies, the only feature that can reliably be measured in the full sample. A more detailed analysis of the extreme objects with high quality rest-frame UV spectra will be presented separately.

3. INFERENCES FROM REST-FRAME OPTICAL EMISSION LINES

As shown in Figure 1, the extreme sample lies in the upper left corner of the BPT diagram. The 14 extreme galaxies have mean (median) stellar mass 6.2×10^9 (4.0×10^9) M_\odot , and mean (median) dust-corrected H α star formation rate 36.6 (27.8) $M_\odot \text{ yr}^{-1}$ (see Table 1; star formation rates are calculated assuming the Kennicutt (1998) relationship between SFR and H α luminosity). Their median rest-frame UV absolute magnitude is $M_{\text{UV}} = -20.66$, indicating that these are L^* galaxies; Reddy & Steidel (2009) find $M^* = -20.70$ at $z \sim 2$, and all of the extreme objects are within ~ 1 mag of this value.

We show several other galaxy samples in Figure 1 for comparison. The $z \sim 2$ KBSS parent sample of Steidel et al. (2014) is shown in red. With the extreme galaxies excluded, the KBSS galaxies are similar to the extreme sample in mass and SFR, with a somewhat higher mean (median) mass of 2.0×10^{10} (9.7×10^9) M_\odot and slightly lower mean (median) SFR of 36.1 (23.6) $M_\odot \text{ yr}^{-1}$. Stellar masses are computed by modeling the spectral energy distribution from the rest-frame UV to near-IR, with

broadband magnitudes corrected for the contribution of nebular emission lines. We use the Bruzual & Charlot (2003) stellar population models with solar metallicity, the Calzetti et al. (2000) extinction law, and assume a constant star formation history; detailed descriptions of the modeling procedure and discussions of the systematic uncertainties associated with these choices are given by Shapley et al. (2005) and Reddy et al. (2012).

We also show ten local “Green Pea” galaxies in green (Henry et al. 2015), and contours showing the locus of Sloan Digital Sky Survey galaxies in grey. The Green Peas are drawn from the SDSS, with selection based on very high equivalent width rest-frame optical emission lines (Cardamone et al. 2009; Izotov et al. 2011). The ten Green Peas shown are somewhat lower in mass and SFR than the extreme $z \sim 2$ sample, with median stellar mass and SFR $1.0 \times 10^9 M_\odot$ and $15.2 M_\odot \text{ yr}^{-1}$ respectively. The extreme sample lies in a region of the BPT diagram in which there are relatively few local galaxies; however, six of the ten Green Peas fall within the extreme selection box, and only one is > 0.1 dex from the extreme cuts in either $[\text{N II}]/\text{H}\alpha$ or $[\text{O III}]/\text{H}\beta$. We mark the Green Peas that meet the extreme BPT selection criteria with open circles in later figures.

We estimate the metallicity of the extreme galaxies using the O3N2 indicator proposed by Pettini & Pagel (2004), which Steidel et al. (2014) show to be in reasonable agreement with metallicities derived from the T_e method (using the $[\text{O III}] \lambda\lambda 1661, 1666$ auroral lines) for three of the galaxies in the extreme sample. This calibration has the advantage of using only closely spaced pairs of emission lines, and is therefore insensitive to uncertainties in band-to-band calibration or reddening; however, because we report 3σ upper limits on $[\text{N II}]$ for half of the sample, we determine upper limits on metallicity for 7/14 galaxies.

If we count upper limits as detections, the extreme sample occupies a narrow range in metallicity, with $12 + \log(\text{O}/\text{H})$ ranging from 7.85 to 8.12 and mean (median) oxygen abundance 8.03 (8.06). For comparison, the $z \sim 2$ sample of Steidel et al. (2014), not including the 14 extreme galaxies, has mean (median) O3N2 metallicity 8.29 (8.27), again counting $[\text{N II}]$ limits as detections.

The metallicities of the extreme $z \sim 2$ sample are very similar to the T_e -based metallicities of the Green Pea comparison sample, which range from 7.86 to 8.17 and have an identical mean of 8.03 (Izotov et al. 2011; Henry et al. 2015). We use this Green Pea sample to assess the reliability of the O3N2 indicator by comparing the O3N2 metallicities of the Green Peas with their direct abundances measured from the $[\text{O III}] \lambda 4363$ line. We find that the O3N2 metallicities are lower than the T_e metallicities by 0.06 dex on average, seven of the ten Green Peas agree within 0.1 dex, and only one object disagrees by > 0.2 dex; this object is also the farthest from the extreme selection box in the BPT diagram by a considerable margin. We conclude that for galaxies in this range of parameter space, the O3N2 diagnostic appears to be a reliable indicator of the gas phase oxygen abundance.

The similar metallicities of the extreme galaxies are a consequence of the selection criteria, since each point on the $[\text{O III}]/\text{H}\beta$ vs. $[\text{N II}]/\text{H}\alpha$ diagram directly corresponds to a metallicity determined with the O3N2 indi-

cator. In this sense, the extreme sample is metallicity-selected. The oxygen abundances of the extreme sample are listed in Table 1.

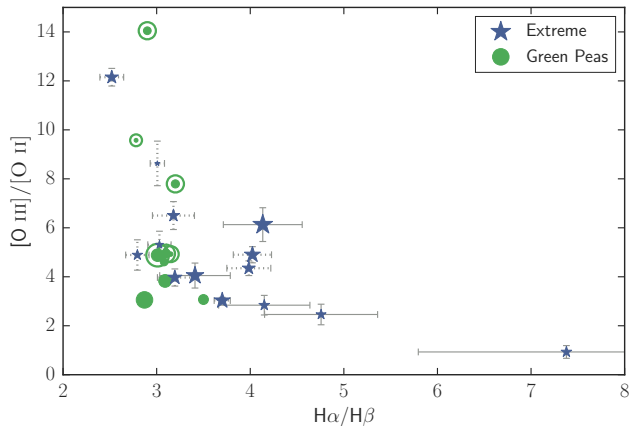


FIG. 2.— The extinction-corrected $[\text{O III}] \lambda\lambda 4959, 5007/[\text{O II}] \lambda\lambda 3727, 3729$ ratio vs. $\text{H}\alpha/\text{H}\beta$ for the extreme and Green Pea samples. We identify the extreme galaxies with Balmer decrements measured with $> 10\sigma$ significance with dashed error bars; the five objects with $\text{H}\alpha/\text{H}\beta$ ratios measured with less than 10σ significance are marked with solid error bars. Green Peas which meet the extreme BPT selection criteria are circled. The sizes of the symbols increase with increasing $\text{Ly}\alpha$ equivalent width (see Section 4).

We also use the nebular line measurements to assess the extinction and ionization properties of the extreme sample, from the $\text{H}\alpha/\text{H}\beta$ and $[\text{O III}]/[\text{O II}]$ ratios respectively. Both of these ratios employ measurements made in two different bands (the H and J bands for $[\text{O III}]$ and $[\text{O II}]$, and the K and H bands for $\text{H}\alpha$ and $\text{H}\beta$). Band-to-band corrections for slit losses (based on stars placed on each mask, modeling of the line profiles, comparison of the spectroscopic continuum to broadband photometry, and multiple observations of the same objects) have been applied, but these ratios are subject to larger systematic uncertainties than the ratios of closely spaced lines such as $[\text{O III}]/\text{H}\beta$ and $[\text{N II}]/\text{H}\alpha$. The median correction is a factor of 2 in all three bands, with a median uncertainty of 6%; all H - and K -band corrections have $< 20\%$ uncertainties, as do all but two of the J -band corrections (Q0821-BX102 and Q1700-BX553 have 27% and 28% uncertainties respectively). The slit-loss corrections are discussed in full elsewhere (Steidel et al. 2014; Strom et al. in preparation). $\text{H}\beta$ fluxes are also corrected for underlying absorption by a factor of 1.06.

The $\text{H}\alpha/\text{H}\beta$ ratios of the extreme sample and their statistical errors are listed in Table 1. In contrast to the Green Peas, which lie close to the Case B value¹¹ with mean and standard deviation $\langle \text{H}\alpha/\text{H}\beta \rangle = 3.07 \pm 0.19$, the extreme galaxies show considerable variation in $\text{H}\alpha/\text{H}\beta$, with half of the sample having $\text{H}\alpha/\text{H}\beta > 3.5$. We find mean and standard deviation $\langle \text{H}\alpha/\text{H}\beta \rangle = 3.80 \pm 1.16$, with values ranging from below Case B to a maximum of 7.38. However, we note that the objects with the highest

$\text{H}\alpha/\text{H}\beta$ ratios have the largest uncertainties. The reliability of the Balmer decrement measurements will be discussed in detail in a forthcoming paper (Strom et al. 2016, in prep); here, we note that Strom et al. find that extinction corrections for galaxies with measurements of the Balmer decrement with less than 10σ significance are less reliable than those with higher S/N.¹² We therefore adopt this threshold in considering whether our $\text{H}\alpha/\text{H}\beta$ measurements are robust. Nine of the 14 extreme galaxies have $> 10\sigma$ Balmer decrement measurements, and we find lower extinction in this more robust subsample, with mean (median) $\text{H}\alpha/\text{H}\beta = 3.27$ (3.18) and standard deviation 0.49. These results suggest that the extreme $z \sim 2$ galaxies have a somewhat wider range in nebular line extinction than the Green Peas, but a larger sample with very high S/N Balmer decrement measurements is required in order to confirm and quantify this result.

We estimate the ionization states of the extreme and Green Pea samples via the $[\text{O III}]/[\text{O II}]$ ratio, which increases with increasing ionization parameter with some additional dependence on metallicity (e.g. Kewley & Dopita 2002). We measure $\text{O}_{32} \equiv F([\text{O III}] \lambda\lambda 4959, 5007)/F([\text{O II}] \lambda\lambda 3727, 3729)$. The observed $[\text{O III}]/[\text{O II}]$ ratios of the extreme galaxies are listed in Table 1; values range between 2.4 and 12.2, with a median value of 5.2. We then correct the $[\text{O III}]/[\text{O II}]$ ratios for extinction, using the Balmer decrement measurements and the Cardelli et al. (1989) extinction law with $R_V = 3.1$. The median extinction-corrected $[\text{O III}]/[\text{O II}]$ ratio is 4.6, while the extreme galaxies with $> 10\sigma$ Balmer decrements have median 4.9. These values are significantly higher than those of more typical star-forming galaxies at the same redshift; for the parent KBSS sample, Strom et al. (in prep) find median $\text{O}_{32} = 1.7$ for galaxies with $> 10\sigma$ measurements of the Balmer decrement (and median $\text{O}_{32} = 1.4$ for the full sample), while Sanders et al. (2015) use a sample of $z \sim 2.3$ galaxies from the MOSDEF survey (Kriek et al. 2015) and find median $\text{O}_{32} = 1.3$, with a 68% upper bound of 2.3. As expected, the extreme line ratio criteria identify highly ionized galaxies at $z \sim 2$.

The extreme galaxies have $[\text{O III}]/[\text{O II}]$ ratios similar to the Green Peas: the ten galaxies studied by Henry et al. (2015) have median $\text{O}_{32} = 4.9$, while the subset that meet the extreme BPT selection criteria have median $\text{O}_{32} = 6.4$. The Green Peas are also much more highly ionized than typical galaxies in the local universe; Sanders et al. (2015) report median $\text{O}_{32} = 0.3$ for their $0.04 < z < 0.1$ SDSS comparison sample.

The extinction-corrected $[\text{O III}]/[\text{O II}]$ ratios are plotted against $\text{H}\alpha/\text{H}\beta$ for both the extreme sample and the Green Peas in Figure 2. The Green Peas and most of the extreme galaxies with $> 10\sigma$ Balmer decrement measurements occupy a similar region in this diagram, but the extreme sample shows a lower S/N tail of objects with high $\text{H}\alpha/\text{H}\beta$ and low $[\text{O III}]/[\text{O II}]$. Because the extinction corrections for these objects are more uncertain, it is not yet clear whether the low $[\text{O III}]/[\text{O II}]$ ratios are

¹¹ In this work we adopt an intrinsic ratio $I(\text{H}\alpha)/I(\text{H}\beta) = 2.89$, which Steidel et al. (2016, in prep) find is predicted by photoionization models that best reproduce the observed line ratios of a subsample of KBSS galaxies with high quality rest-frame UV and optical spectra.

¹² This determination is based on the finding that galaxies with extinction corrections based on a $> 10\sigma$ measurement of the Balmer decrement form a tight sequence in the dust-corrected O_{32} - R_{23} plane, while many objects with less significant $\text{H}\alpha/\text{H}\beta$ measurements are outliers, likely due to an error in the extinction correction.

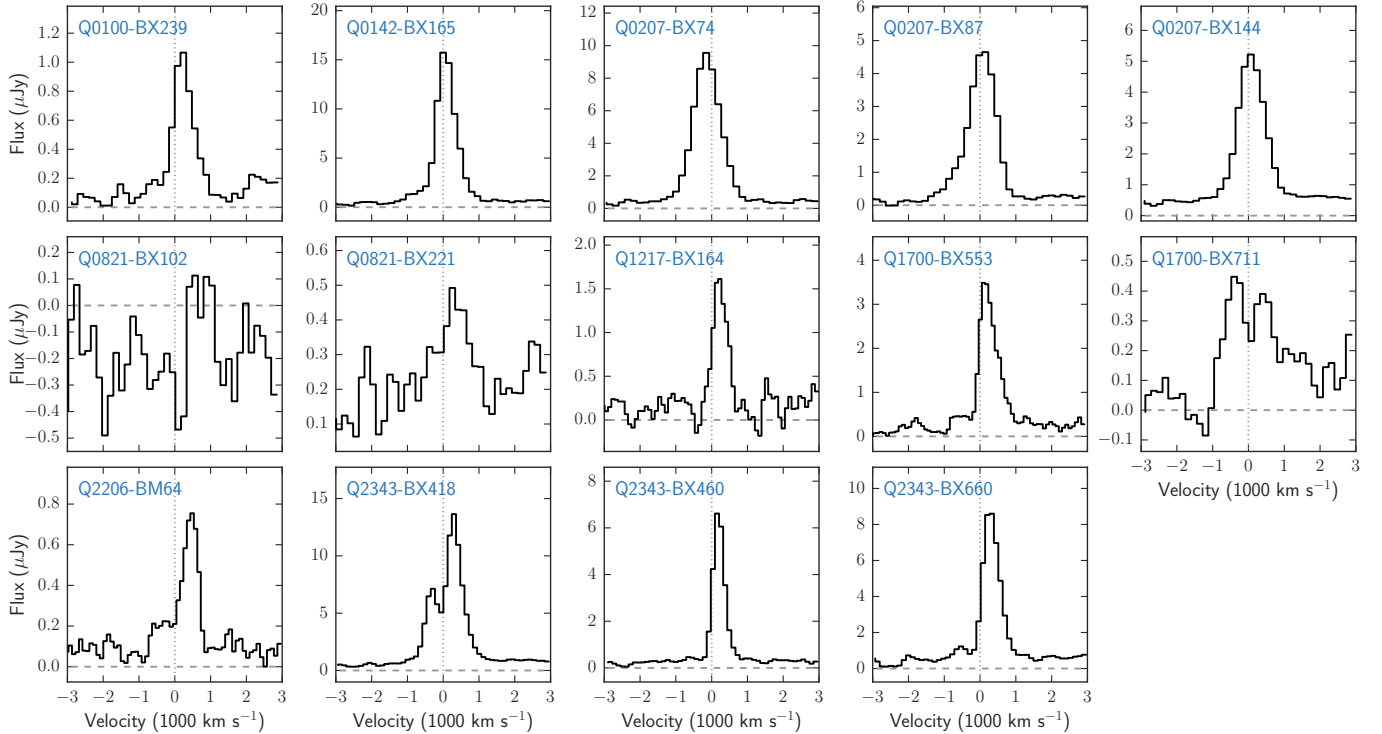


FIG. 3.— Ly α profiles of the 14 extreme galaxies. Vertical dotted lines show the systemic redshift measured from nebular emission lines. Most of the extreme galaxies show strong Ly α emission.

due to an overestimate of the extinction. It is also notable that the extreme BPT selection criteria identify the Green Peas with the highest values of O_{32} .

We conclude from these nebular line measurements that the extreme selection reliably identifies galaxies with low ($\sim 20\%$ of solar) metallicities and ionization states consistently higher than those of more typical $z \sim 2$ galaxies. The extreme galaxies also have less dust attenuation at Ly α than more typical $z \sim 2$ galaxies; however, there is considerable range in the $H\alpha/H\beta$ ratio, and a more robust measurement of the variation in extinction requires a larger sample with high S/N measurements of the Balmer decrement. We discuss the nebular emission line properties of the extreme sample further in the context of the Ly α measurements described below.

4. Ly α PROPERTIES

The Ly α profiles of the 14 extreme galaxies are shown in Figure 3, from which it is clear that most of the galaxies in the sample show Ly α in emission. The exceptions are the two galaxies Q0821-BX102 and Q0821-BX221, which have weak or no emission. BX221 has the lowest SFR in the sample, though only slightly; otherwise these objects appear similar to the rest of the extreme sample. Among the remaining 12 galaxies with strong emission, the lines show a variety of spectral morphologies: most are strong and relatively symmetric, while a few show multiple components. This diversity is consistent with previous observations of galaxies with strong Ly α emission (e.g. Kulas et al. 2012; Chonis et al. 2013; Erb et al. 2014; Trainor et al. 2015).

At the moderately low spectral resolution of our observations, Q2343-BX418 (measured with $\sim 300 \text{ km s}^{-1}$ resolution) and Q1700-BX711 (measured with $\sim 500 \text{ km s}^{-1}$ resolution) show double peaks: the red peak is signifi-

cantly stronger in BX418, while BX711 has a slightly stronger blue peak and may have multiple components of redshifted emission. Q2206-BM64 also shows emission blueward of zero velocity. These objects are not outliers among any of the properties we measure in this work, indicating that the Ly α emission profile depends in part on factors which are not reflected by the nebular line ratios. We will explore this issue further with a detailed analysis of the highest S/N rest-frame UV spectra in the extreme sample, focusing on the interstellar absorption lines as well as on Ly α (Erb et al. in prep).

We measure Ly α fluxes and equivalent widths following the procedure described by Kornei et al. (2010), in which each line profile is classified as emission, absorption, combination or noise, the continuum levels on the red and blue sides of the line are determined separately, and the equivalent width is calculated to be the flux in the line divided by the red continuum level. Uncertainties are determined via Monte Carlo simulations in which each spectrum is perturbed 500 times by a random value drawn from a Gaussian distribution with width corresponding to the uncertainty at each pixel. We repeat the flux and equivalent width measurements for each perturbed spectrum, and the medians and standard deviations of these measurements are taken as the flux, equivalent width, and their uncertainties. For the extreme sample, all galaxies are classified as emission, with the exception of Q0821-BX102 which is classified as noise.

The resulting distribution of Ly α rest-frame equivalent widths is shown in Figure 4, and Ly α measurements are given in Table 2. The mean (median) Ly α equivalent width of the extreme sample is 39.3 (35.6) Å, and 11 of the 14 galaxies (79%) have $W_{\text{Ly}\alpha} > 20$ Å, the nominal threshold to be classified as an LAE, while an additional

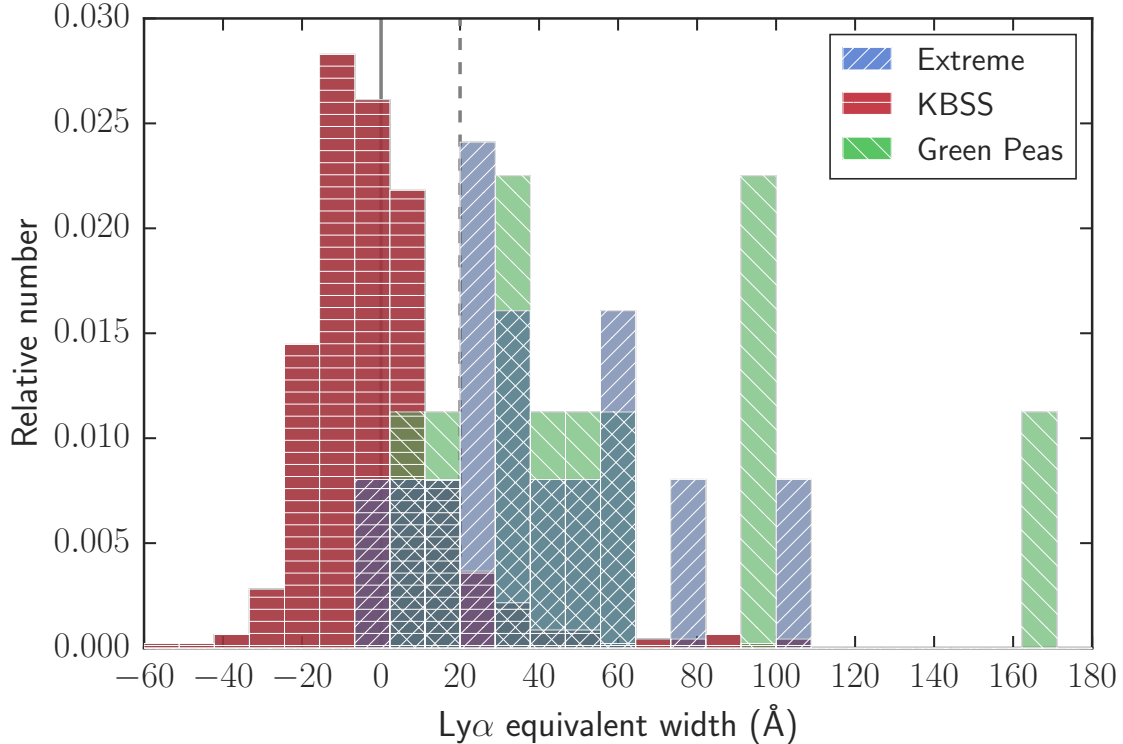


FIG. 4.— $\text{Ly}\alpha$ rest-frame equivalent width distributions for the extreme sample (blue), 522 $2.0 \leq z \leq 2.6$ galaxies from the KBSS parent sample (red), and Green Pea galaxies (green, Henry et al. 2015). Histograms are normalized to an integral of unity. The extreme and Green Pea samples show similar $W_{\text{Ly}\alpha}$ distributions, while the KBSS comparison sample typically shows much weaker $\text{Ly}\alpha$ emission.

object has $W_{\text{Ly}\alpha} = 18.0 \pm 2.0 \text{ \AA}$.

We show two other galaxy samples in Figure 4 for comparison. The dark red histogram shows the $\text{Ly}\alpha$ equivalent width distribution of 522 UV-selected KBSS galaxies at $2.0 \leq z \leq 2.6$ with mean redshift $\langle z \rangle = 2.28 \pm 0.16$. These galaxies were selected without regard to their nebular line ratios, and equivalent widths were measured using the same procedure as for the extreme sample, with $\text{Ly}\alpha$ spectral morphologies independently classified by three of the authors (DKE, NAR, AES). The mean (median) $\text{Ly}\alpha$ equivalent width of this comparison sample is -1.0 (-4.4) \AA , and 9% of the galaxies in the sample qualify as LAEs with $W_{\text{Ly}\alpha} > 20 \text{ \AA}$. A two sample K-S test indicates that the extreme and KBSS comparison samples are statistically different: the probability that the two samples are drawn from the same equivalent width distribution is $P = 8.0 \times 10^{-8}$ (5.4σ significance).

We also compare the equivalent widths of the Green Pea galaxies (Henry et al. 2015; green histogram). In contrast to the KBSS sample, the extreme $z \sim 2$ galaxies and the Green Peas have similar equivalent width distributions; the mean (median) $W_{\text{Ly}\alpha}$ of the Green Peas is 59.6 (44.0) \AA , and a K-S test finds that the probability that the extreme $z \sim 2$ galaxies and the Green Peas are drawn from the same distribution of equivalent widths is $P = 0.59$ (0.54σ significance).

Finally, we measure the offset of the centroid of the $\text{Ly}\alpha$ emission line¹³ from the systemic velocity, finding a

mean (median) velocity offset of 186 (208) km s^{-1} . This offset is typical of LAEs at $z \sim 2$, which generally have smaller velocity offsets than continuum-selected galaxies at the same redshifts (Hashimoto et al. 2013; Shibuya et al. 2014; Erb et al. 2014; Trainor et al. 2015); similarly, continuum-selected $z \sim 3$ galaxies with strong $\text{Ly}\alpha$ emission show smaller velocity differences between the interstellar absorption lines and $\text{Ly}\alpha$ than galaxies with lower $\text{Ly}\alpha$ equivalent widths (Shapley et al. 2003).

These comparisons clearly show that galaxy selection via nebular emission line properties can yield a high fraction of objects with strong $\text{Ly}\alpha$ emission. Previous studies of small samples of relatively bright LAEs have indicated that galaxies with strong $\text{Ly}\alpha$ emission tend to have low metallicities (Nakajima et al. 2013; Song et al. 2014); we now see that the reverse is also true, reinforcing the connection between the physical conditions in H II regions and the escape of $\text{Ly}\alpha$ photons.

4.1. $\text{Ly}\alpha$ Emission and Extinction

Many studies have shown that galaxies with strong $\text{Ly}\alpha$ emission have relatively low extinction, as measured either from their bluer UV slopes or lower $\text{H}\alpha/\text{H}\beta$ ratios (e.g. Shapley et al. 2003; Gawiser et al. 2006; Vanzella et al. 2009; Kornei et al. 2010; Pentericci et al. 2010; Guaita et al. 2011; Atek et al. 2014; McLinden et al. 2014; Henry et al. 2015, cf. Hagen et al. 2016). The extreme $z \sim 2$ sample shows a range in the Balmer decrement, suggesting some range in internal extinction.

As discussed in Section 3 above, we use the Cardelli individual components of the $\text{Ly}\alpha$ emission.

¹³ Velocity offsets are measured from the flux-weighted centroid of the total $\text{Ly}\alpha$ emission in all cases. A forthcoming analysis of objects with higher S/N spectra will address the velocities of

et al. (1989) extinction law to calculate $E(B - V)_{\text{neb}}$ for the extreme sample. The 14 galaxies have median $\text{H}\alpha/\text{H}\beta = 3.56$ with a standard deviation of 1.16, which results in median $E(B - V)_{\text{neb}} = 0.20 \pm 0.23$. If we consider only the subsample with $> 10\sigma$ measurements of the Balmer decrement, we find median $\text{H}\alpha/\text{H}\beta = 3.18$ and $E(B - V)_{\text{neb}} = 0.09$. For comparison, Steidel et al. (2014) report median $\text{H}\alpha/\text{H}\beta = 3.89 \pm 0.65$ for the KBSS parent sample, for a corresponding color excess of $E(B - V)_{\text{neb}} = 0.28 \pm 0.16$. These values indicate that the median extinction at the wavelength of Ly α is lower in the extreme sample than in the KBSS comparison sample; it is 1.9 times lower when we compare the full extreme sample, and 4.3 times lower if only the $> 10\sigma$ extreme sample is used.

Measurements of extinction from SED fitting (adopting the Calzetti et al. 2000 extinction law) also indicate lower attenuation at Ly α in the extreme sample relative to the KBSS comparison sample, although the difference is smaller. The extreme objects have median $E(B - V)_{\text{cont}} = 0.11$, while the comparison sample has median $E(B - V)_{\text{cont}} = 0.17$. This difference corresponds to a factor of 1.6 lower attenuation at Ly α in the extreme sample.

The Green Pea galaxies, which are similar to the extreme sample in their metallicities and Ly α equivalent widths, have uniformly low extinction, with median $\text{H}\alpha/\text{H}\beta = 3.07$. This is roughly comparable to the $> 10\sigma$ extreme sample, which has 1.3 times higher median extinction at Ly α ; if the full extreme sample is used, we find that the median extinction at Ly α is 2.9 times higher for the extreme galaxies than for the Green Peas. The $\text{H}\alpha/\text{H}\beta$ ratios for both the extreme sample and the Green Peas are shown in Figure 2, plotted against the extinction-corrected $[\text{O III}]/[\text{O II}]$ ratio. The symbol sizes are scaled by the Ly α equivalent width, from which it is apparent that the strength of Ly α emission is uncorrelated with both the Balmer decrement and O_{32} .

We conclude that the lower extinction of the extreme galaxies relative to the KBSS parent sample likely facilitates the escape of Ly α photons, but some of the extreme objects may have both moderate to high extinction and strong Ly α emission. This combination is not surprising; although most galaxies with strong Ly α emission have little dust, Kornei et al. (2010) and Hagen et al. (2014) find LAEs with $E(B - V)$ up to 0.3 and 0.4 respectively. It is perhaps more unexpected for low metallicity objects with line ratios similar to the Green Peas to show significant extinction, and we await higher S/N measurements of the Balmer decrement to confirm whether this is indeed the case.

4.2. The Ly α Escape Fraction

We estimate the fraction of Ly α photons reaching the detector from the Ly $\alpha/\text{H}\alpha$ flux ratio, assuming an intrinsic ratio of $\text{Ly}\alpha/\text{H}\alpha = 8.7$ (Henry et al. 2015; Trainor et al. 2015) and correcting the H α fluxes for extinction as described in Section 4.1 above. The UV spectra are corrected for slit losses by normalizing to the G -band magnitude; as discussed below, this does not account for additional losses in Ly α due to possible differences in spatial distribution relative to the continuum. The H α fluxes are also corrected for slit losses, as we describe in Section 3 above. We find that the escape fraction is

typically low, with mean and median values of 0.08; the largest value in the sample is 0.27. These escape fractions are listed in Table 2 and plotted vs. Ly α equivalent width in Figure 5.

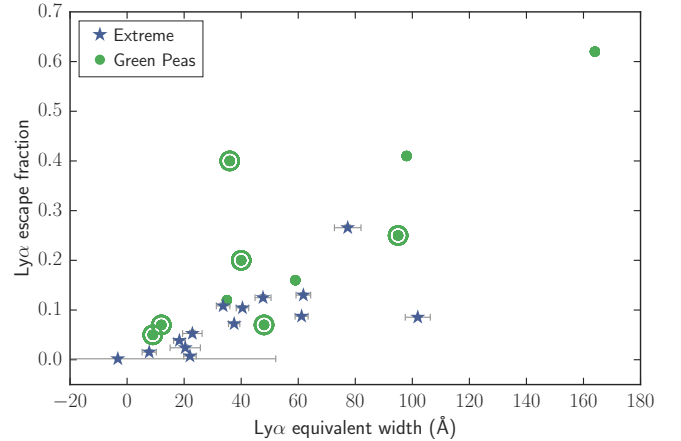


FIG. 5.— The Ly α escape fraction vs. the Ly α equivalent width for the extreme and Green Pea samples. For both samples, the escape fractions shown are not corrected for the fraction of Ly α photons which escape the spectroscopic aperture; see discussion in text. Green Peas which meet the extreme selection criteria in the BPT diagram are circled.

For larger populations of star-forming galaxies at $z \sim 2$, Steidel et al. (2011) and Hayes et al. (2010) find Ly α escape fractions of $\sim 5\%$, while Ciardullo et al. (2014) find $f_{\text{esc}}^{\text{Ly}\alpha} < 6\%$, only slightly lower than our mean value of 0.08. LAEs typically have higher escape fractions: Hayes et al. (2010) and Steidel et al. (2011) find $f_{\text{esc}}^{\text{Ly}\alpha} \sim 0.3$ for the LAEs in their samples, and Trainor et al. (2015) also estimate an escape fraction of $\sim 30\%$ for a sample of faint LAEs at $z \sim 2.7$. However, in contrast to the current work, all of these studies measure Ly α fluxes from either narrow-band imaging or integral field spectroscopy and are therefore not subject to aperture losses from the spectroscopic slit. A variety of recent results have shown that galaxies at both high and low redshifts are surrounded by diffuse halos of Ly α emission (Steidel et al. 2011; Matsuda et al. 2012; Feldmeier et al. 2013; Hayes et al. 2013; Momose et al. 2014, 2016). For UV-selected galaxies comparable to those in the current sample, Steidel et al. (2011) find that spectroscopic Ly α fluxes are ~ 5 times lower than fluxes measured from narrow-band images on average, and ~ 3 times lower for LAEs. For a sample of fainter LAEs, Trainor et al. (2015) find a smaller factor of ~ 2 correction.

We have no way to measure the fraction of Ly α photons which are not captured by the slit for the extreme galaxies, but we can estimate the appropriate correction by considering other galaxy samples. The UV-continuum-selected LAEs of Steidel et al. (2011) are comparable to the extreme sample in continuum luminosity and strength of Ly α emission, while the LAEs studied by Trainor et al. (2015) occupy the extreme region in the BPT diagram (Trainor et al., in prep); these results suggest that a factor of 2–3 correction is likely to be appropriate for the extreme sample.

We can also estimate the size of this correction using the results of Momose et al. (2016), who measure

extended Ly α halos around a large sample of LAEs at $z = 2.2$. They find that the total Ly α luminosity ranges from ~ 2 –4 times the luminosity within an aperture $1''$ in radius, and that the fraction in the extended halo depends on both Ly α luminosity and equivalent width, with lower luminosity galaxies with lower equivalent widths having a higher fraction of flux in the halo. Our extreme sample spans nearly the full range in Ly α luminosity and equivalent width considered by Momose et al. (2016), but comparing our median luminosity and equivalent widths with their results suggest that the factor of 2–3 correction determined above is reasonable. Adjusting our escape fractions by this factor then results in a mean value of 0.16–0.24, somewhat lower than or roughly comparable to other samples of LAEs.

The COS aperture used to measure the Ly α emission of the Green Peas and the $1.2''$ slit used at $z \sim 2$ span similar physical sizes of 8–10 kpc, much larger than the typical sizes of both samples; both the Green Peas and UV-selected $z \sim 2$ galaxies with strong Ly α emission have rest-frame UV sizes $r \lesssim 2$ kpc (Henry et al. 2015; Law et al. 2012). However, when aperture corrections are not applied the Ly α escape fractions of the Green Peas are higher than those of the extreme sample, with mean (median) $f_{\text{esc}}^{\text{Ly}\alpha} = 0.24$ (0.18) compared to the extreme mean of 0.08. This difference may in part be accounted for by higher extinction at Ly α in the higher redshift sample, given the well-studied correlation between $E(B - V)$ and Ly α equivalent width (see Section 4.1 above). The $z \sim 2$ galaxies may also be subject to larger aperture losses; while only three of the Green Peas have larger aperture Ly α measurements (either from *GALEX* or from the Ly α Reference Sample, Östlin et al. 2014; Hayes et al. 2014) which can be compared with the COS spectra, the COS aperture captures 40–75% of the total flux for these three objects, somewhat larger than the ~ 30 –50% we have estimated for the extreme sample.

While the extreme galaxies have higher aperture-corrected Ly α escape fractions than more typical star-forming galaxies at the same redshifts, the typical escape fraction remains relatively low; as in all other galaxy samples studied, the Ly α photons of these relatively low metallicity objects are subject to significant scattering and absorption.

5. SUMMARY AND DISCUSSION

Motivated by previous observations of strong Ly α emission in low metallicity galaxies at $z \sim 2$ (Erb et al. 2010; Stark et al. 2014), we study the Ly α properties of a sample of 14 galaxies lying in the upper left corner of the [O III] $\lambda 5007$ /H β vs. [N II] $\lambda 6584$ /H α diagnostic diagram, at the low metallicity/high ionization end of the star-forming sequence (see Figure 1). This cut is effectively a metallicity selection, as we use the O3N2 diagnostic to determine oxygen abundances, and the galaxies in this extreme sample have typical metallicities of $12 + \log(\text{O}/\text{H}) \sim 8.0$. The extreme galaxies have median stellar mass $4.0 \times 10^9 M_{\odot}$, and median dust-corrected H α star formation rate $27.8 M_{\odot} \text{ yr}^{-1}$. Their median rest-frame UV absolute magnitude is $M_{\text{UV}} = -20.66$, comparable to M^* at $z \sim 2$ (-20.70 , Reddy & Steidel 2009).

The mean (median) rest-frame Ly α equivalent width

of this extreme galaxy sample is 39.3 (35.6) Å, and 11 of the 14 objects (79%) are Ly α -emitters (LAEs) with $W_{\text{Ly}\alpha} > 20$ Å. This is a much higher LAE fraction than that of a comparable sample of 522 star-forming galaxies at $2.0 < z < 2.6$ selected without regard to their nebular line ratios. This comparison sample has mean (median) Ly α equivalent width -1.0 (-4.4) Å, and 9% of the comparison galaxies qualify as LAEs. Although the Ly α equivalent width distribution of the extreme galaxies is quite different than that of more typical star-forming galaxies at $z \sim 2$, it is similar to that of the local Green Pea galaxies, $z \sim 0.2$ galaxies from the Sloan Digital Sky Survey selected to have very high equivalent width [O III] emission. The Ly α profiles are shown in Figure 3, and the equivalent width distributions of the extreme galaxies and comparison samples are shown in Figure 4.

The galaxies in the extreme sample show a range in nebular extinction as estimated from the H α /H β ratio (see Figure 2). The median attenuation at Ly α is 1.9 times lower than that of the KBSS parent sample, and 4.3 times lower if only the objects with the most robust measurements of the Balmer decrement are considered. This difference in extinction undoubtedly aids the escape of Ly α photons in the extreme galaxies, but the range in H α /H β ratios suggests that moderate extinction is not a barrier to strong Ly α emission. This result is not surprising, as some LAEs are known to be dusty (Kornei et al. 2010; Hagen et al. 2014), although it may be more unexpected for low metallicity objects with line ratios similar to the nearly dust-free Green Peas to show significant extinction. Future higher S/N measurements of the Balmer decrement will determine whether or not this is indeed the case.

The median oxygen abundance of the extreme galaxies is $\sim 50\%$ lower than that of the parent sample, and this may also facilitate the escape of Ly α photons, as the harder ionizing spectrum and higher ionization parameter associated with strong, low metallicity star formation may reduce the covering fraction or column density of neutral hydrogen (e.g. Nakajima et al. 2013; Shibuya et al. 2014; Erb et al. 2014; Henry et al. 2015; Trainor et al. 2015). We will explore this question further with a detailed analysis of the interstellar absorption lines and Ly α profile structure of the extreme galaxies with high S/N rest-frame UV spectra (Erb et al. in prep).

The high fraction of LAEs in the extreme galaxy sample indicates that the use of nebular emission line ratios can be an effective technique for identifying samples of galaxies which are likely to have strong Ly α emission. This method may be particularly useful at redshifts at which Ly α is not otherwise accessible; in particular, future observations of nebular emission line ratios at $z \gtrsim 6$ with *JWST* may allow the identification of galaxies that are likely to have a sufficiently low column density or covering fraction of neutral hydrogen to permit the escape of Ly α photons (and, potentially, Lyman continuum radiation as well), even if the opacity of the intergalactic medium prevents observation of the Ly α emission directly.

We expect that studies of larger samples of galaxies with extreme line ratios at a range of redshifts will clarify the relationships between the physical conditions in H II regions and the properties that ease the escape of Ly α

and LyC radiation; such an improved understanding will be required in order to fully explain the sources of the photons which reionized the universe.

We would like to thank the anonymous referee for a helpful and constructive report. DKE is supported by the US National Science Foundation through the Faculty Early Career Development (CAREER) Program, grant AST-1255591. Additional support comes from the NSF through grants AST-0908805 (CCS) and AST-1313472

(CCS, ALS), and an NSF Graduate Student Research Fellowship (ALS). We are grateful to Alaina Henry for providing flux measurements for the Green Pea galaxies, and to the organizers and participants of the First Carnegie Symposium in Honor of Leonard Searle, “Understanding Nebular Emission in High-Redshift Galaxies,” held at the Carnegie Observatories in July 2015, for many useful discussions. Finally, we wish to extend thanks to those of Hawaiian ancestry on whose sacred mountain we are privileged to be guests.

REFERENCES

- Atek, H., Kunth, D., Schaerer, D., Mas-Hesse, J. M., Hayes, M., Östlin, G., & Kneib, J.-P. 2014, *A&A*, 561, A89
- Baldwin, J. A., Phillips, M. M., & Terlevich, R. 1981, *PASP*, 93, 5
- Bruzual, G. & Charlot, S. 2003, *MNRAS*, 344, 1000
- Calzetti, D., Armus, L., Bohlin, R. C., Kinney, A. L., Koornneef, J., & Storchi-Bergmann, T. 2000, *ApJ*, 533, 682
- Cardamone, C., Schawinski, K., Sarzi, M., Bamford, S. P., Bennert, N., Urry, C. M., Lintott, C., Keel, W. C., Parejko, J., Nichol, R. C., Thomas, D., Andreescu, D., Murray, P., Raddick, M. J., Slosar, A., Szalay, A., & Vandenberg, J. 2009, *MNRAS*, 399, 1191
- Cardelli, J. A., Clayton, G. C., & Mathis, J. S. 1989, *ApJ*, 345, 245
- Chabrier, G. 2003, *PASP*, 115, 763
- Chonis, T. S., Blanc, G. A., Hill, G. J., Adams, J. J., Finkelstein, S. L., Gebhardt, K., Kollmeier, J. A., Ciardullo, R., Drory, N., Gronwall, C., Hagen, A., Overzier, R. A., Song, M., & Zeimann, G. R. 2013, *ApJ*, 775, 99
- Ciardullo, R., Zeimann, G. R., Gronwall, C., Gebhardt, H., Schneider, D. P., Hagen, A., Malz, A. I., Blanc, G. A., Hill, G. J., Drory, N., & Gawiser, E. 2014, *ApJ*, 796, 64
- Cowie, L. L., Barger, A. J., & Hu, E. M. 2011, *ApJ*, 738, 136
- Dijkstra, M. 2014, *PASA*, 31, e040
- Erb, D. K., Pettini, M., Shapley, A. E., Steidel, C. C., Law, D. R., & Reddy, N. A. 2010, *ApJ*, 719, 1168
- Erb, D. K., Steidel, C. C., Trainor, R. F., Bogosavljević, M., Shapley, A. E., Nestor, D. B., Kulas, K. R., Law, D. R., Strom, A. L., Rudie, G. C., Reddy, N. A., Pettini, M., Konidaris, N. P., Mace, G., Matthews, K., & McLean, I. S. 2014, *ApJ*, 795, 33
- Feldmeier, J., Hagen, A., Ciardullo, R., Gronwall, C., Gawiser, E., Guaita, L., Hagen, L., Bond, N., Acquaviva, V., Blanc, G., Orsi, A., & Kurczynski, P. 2013, *ArXiv e-prints*
- Gawiser, E., van Dokkum, P. G., Gronwall, C., Ciardullo, R., Blanc, G. A., Castander, F. J., Feldmeier, J., Francke, H., Franx, M., Habertzettl, L., Herrera, D., Hickey, T., Infante, L., Lira, P., Maza, J., Quadri, R., Richardson, A., Schawinski, K., Schirmer, M., Taylor, E. N., Treister, E., Urry, C. M., & Virani, S. N. 2006, *ApJ*, 642, L13
- Guaita, L., Acquaviva, V., Padilla, N., Gawiser, E., Bond, N. A., Ciardullo, R., Treister, E., Kurczynski, P., Gronwall, C., Lira, P., & Schawinski, K. 2011, *ApJ*, 733, 114
- Hagen, A., Ciardullo, R., Gronwall, C., Acquaviva, V., Bridge, J., Zeimann, G. R., Blanc, G. A., Bond, N. A., Finkelstein, S. L., Song, M., Gawiser, E., Fox, D. B., Gebhardt, H., Malz, A. I., Schneider, D. P., Drory, N., Gebhardt, K., & Hill, G. J. 2014, *ApJ*, 786, 59
- Hagen, A., Zeimann, G. R., Behrens, C., Ciardullo, R., Grasshorn, Gebhardt, H. S., Gronwall, C., Bridge, J. S., Fox, D. B., Schneider, D. P., Trump, J. R., Blanc, G. A., Chiang, Y.-K., Chonis, T. S., Finkelstein, S. L., Hill, G. J., Jogee, S., & Gawiser, E. 2016, *ApJ*, 817, 79
- Hashimoto, T., Ouchi, M., Shimasaku, K., Ono, Y., Nakajima, K., Rauch, M., Lee, J., & Okamura, S. 2013, *ApJ*, 765, 70
- Hayes, M., Östlin, G., Duval, F., Sandberg, A., Guaita, L., Melinder, J., Adamo, A., Schaerer, D., Verhamme, A., Orlitová, I., Mas-Hesse, J. M., Cannon, J. M., Atek, H., Kunth, D., Laursen, P., Otf-Floranes, H., Pardy, S., Rivera-Thorsen, T., & Herenz, E. C. 2014, *ApJ*, 782, 6
- Hayes, M., Östlin, G., Schaerer, D., Mas-Hesse, J. M., Leitherer, C., Atek, H., Kunth, D., Verhamme, A., de Barros, S., & Melinder, J. 2010, *Nature*, 464, 562
- Hayes, M., Östlin, G., Schaerer, D., Verhamme, A., Mas-Hesse, J. M., Adamo, A., Atek, H., Cannon, J. M., Duval, F., Guaita, L., Herenz, E. C., Kunth, D., Laursen, P., Melinder, J., Orlitová, I., Otf-Floranes, H., & Sandberg, A. 2013, *ApJ*, 765, L27
- Henry, A., Scarlata, C., Martin, C. L., & Erb, D. 2015, *ApJ*, 809, 19
- Izotov, Y. I., Guseva, N. G., & Thuan, T. X. 2011, *ApJ*, 728, 161
- Izotov, Y. I., Orlitová, I., Schaerer, D., Thuan, T. X., Verhamme, A., Guseva, N. G., & Worseck, G. 2016, *Nature*, 529, 178
- Kennicutt, R. C. 1998, *ARA&A*, 36, 189
- Kewley, L. J. & Dopita, M. A. 2002, *ApJS*, 142, 35
- Kewley, L. J., Dopita, M. A., Sutherland, R. S., Heisler, C. A., & Trevena, J. 2001, *ApJ*, 556, 121
- Kornei, K. A., Shapley, A. E., Erb, D. K., Steidel, C. C., Reddy, N. A., Pettini, M., & Bogosavljević, M. 2010, *ApJ*, 711, 693
- Kriek, M., Shapley, A. E., Reddy, N. A., Siana, B., Coil, A. L., Mobasher, B., Freeman, W. R., de Groot, L., Price, S. H., Sanders, R., Shivaie, I., Brammer, G. B., Momcheva, I. G., Skelton, R. E., van Dokkum, P. G., Whitaker, K. E., Aird, J., Azadi, M., Kassis, M., Bullock, J. S., Conroy, C., Davé, R., Kereš, D., & Krumholz, M. 2015, *ApJS*, 218, 15
- Kuhlen, M. & Faucher-Giguère, C.-A. 2012, *MNRAS*, 423, 862
- Kulas, K. R., Shapley, A. E., Kollmeier, J. A., Zheng, Z., Steidel, C. C., & Hainline, K. N. 2012, *ApJ*, 745, 33
- Law, D. R., Steidel, C. C., Shapley, A. E., Nagy, S. R., Reddy, N. A., & Erb, D. K. 2012, *ApJ*, 759, 29
- Matsuda, Y., Yamada, T., Hayashino, T., Yamauchi, R., Nakamura, Y., Morimoto, N., Ouchi, M., Ono, Y., Umemura, M., & Mori, M. 2012, *MNRAS*, 425, 878
- McLean, I. S., Steidel, C. C., Epps, H., Matthews, K., Adkins, S., Konidaris, N., Weber, B., Aliado, T., Brims, G., Canfield, J., Cromer, J., Fucik, J., Kulas, K., Mace, G., Magnone, K., Rodriguez, H., Wang, E., & Weiss, J. 2010, in *Society of Photo-Optical Instrumentation Engineers (SPIE) Conference Series*, Vol. 7735, Society of Photo-Optical Instrumentation Engineers (SPIE) Conference Series
- McLean, I. S., Steidel, C. C., Epps, H. W., Konidaris, N., Matthews, K. Y., Adkins, S., Aliado, T., Brims, G., Canfield, J. M., Cromer, J. L., Fucik, J., Kulas, K., Mace, G., Magnone, K., Rodriguez, H., Rudie, G., Trainor, R., Wang, E., Weber, B., & Weiss, J. 2012, in *Society of Photo-Optical Instrumentation Engineers (SPIE) Conference Series*, Vol. 8446, Society of Photo-Optical Instrumentation Engineers (SPIE) Conference Series
- McLinden, E. M., Rhoads, J. E., Malhotra, S., Finkelstein, S. L., Richardson, M. L. A., Smith, B., & Tilvi, V. S. 2014, *MNRAS*, 439, 446
- Momose, R., Ouchi, M., Nakajima, K., Ono, Y., Shibuya, T., Shimasaku, K., Yuma, S., Mori, M., & Umemura, M. 2014, *MNRAS*, 442, 110
- . 2016, *MNRAS*, 457, 2318
- Nakajima, K., Ouchi, M., Shimasaku, K., Hashimoto, T., Ono, Y., & Lee, J. C. 2013, *ApJ*, 769, 3
- Oke, J. B., Cohen, J. G., Carr, M., Cromer, J., Dingizian, A., Harris, F. H., Labrecque, S., Lucinio, R., Schaal, W., Epps, H., & Miller, J. 1995, *PASP*, 107, 375

- Östlin, G., Hayes, M., Duval, F., Sandberg, A., Rivera-Thorsen, T., Marquart, T., Orlitová, I., Adamo, A., Melinder, J., Guaita, L., Atek, H., Cannon, J. M., Gruyters, P., Herenz, E. C., Kunth, D., Laursen, P., Mas-Hesse, J. M., Micheva, G., Otf-Floranes, H., Pardy, S. A., Roth, M. M., Schaerer, D., & Verhamme, A. 2014, *ApJ*, 797, 11
- Pentericci, L., Grazian, A., Scarlata, C., Fontana, A., Castellano, M., Giallongo, E., & Vanzella, E. 2010, *A&A*, 514, A64
- Pettini, M. & Pagel, B. E. J. 2004, *MNRAS*, 348, L59
- Reddy, N. A., Pettini, M., Steidel, C. C., Shapley, A. E., Erb, D. K., & Law, D. R. 2012, *ApJ*, 754, 25
- Reddy, N. A. & Steidel, C. C. 2009, *ApJ*, 692, 778
- Robertson, B. E., Ellis, R. S., Furlanetto, S. R., & Dunlop, J. S. 2015, *ApJ*, 802, L19
- Robertson, B. E., Furlanetto, S. R., Schneider, E., Charlot, S., Ellis, R. S., Stark, D. P., McLure, R. J., Dunlop, J. S., Koekemoer, A., Schenker, M. A., Ouchi, M., Ono, Y., Curtis-Lake, E., Rogers, A. B., Bowler, R. A. A., & Cirasuolo, M. 2013, *ApJ*, 768, 71
- Sanders, R. L., Shapley, A. E., Kriek, M., Reddy, N. A., Freeman, W. R., Coil, A. L., Siana, B., Mobasher, B., Shivaee, I., Price, S. H., & de Groot, L. 2015, *ApJ*, 799, 138
- Shapley, A. E., Steidel, C. C., Erb, D. K., Reddy, N. A., Adelberger, K. L., Pettini, M., Barmby, P., & Huang, J. 2005, *ApJ*, 626, 698
- Shapley, A. E., Steidel, C. C., Pettini, M., & Adelberger, K. L. 2003, *ApJ*, 588, 65
- Shibuya, T., Ouchi, M., Nakajima, K., Hashimoto, T., Ono, Y., Rauch, M., Gauthier, J.-R., Shimasaku, K., Goto, R., Mori, M., & Umemura, M. 2014, *ApJ*, 788, 74
- Song, M., Finkelstein, S. L., Gebhardt, K., Hill, G. J., Drory, N., Ashby, M. L. N., Blanc, G. A., Bridge, J., Chonis, T., Ciardullo, R., Fabricius, M., Fazio, G. G., Gawiser, E., Gronwall, C., Hagen, A., Huang, J.-S., Jogee, S., Livermore, R., Salmon, B., Schneider, D. P., Willner, S. P., & Zeimann, G. R. 2014, *ApJ*, 791, 3
- Stark, D. P., Richard, J., Siana, B., Charlot, S., Freeman, W. R., Gutkin, J., Wofford, A., Robertson, B., Amanullah, R., Watson, D., & Milvang-Jensen, B. 2014, *MNRAS*, 445, 3200
- Steidel, C. C., Bogosavljević, M., Shapley, A. E., Kollmeier, J. A., Reddy, N. A., Erb, D. K., & Pettini, M. 2011, *ApJ*, 736, 160
- Steidel, C. C., Rudie, G. C., Strom, A. L., Pettini, M., Reddy, N. A., Shapley, A. E., Trainor, R. F., Erb, D. K., Turner, M. L., Konidaris, N. P., Kulas, K. R., Mace, G., Matthews, K., & McLean, I. S. 2014, *ApJ*, 795, 165
- Steidel, C. C., Shapley, A. E., Pettini, M., Adelberger, K. L., Erb, D. K., Reddy, N. A., & Hunt, M. P. 2004, *ApJ*, 604, 534
- Trainor, R. F., Steidel, C. C., Strom, A. L., & Rudie, G. C. 2015, *ApJ*, 809, 89
- Vanzella, E., de Barros, S., Vasei, K., Alavi, A., Giavalisco, M., Siana, B., Grazian, A., Hasinger, G., Suh, H., Cappelluti, N., Vito, F., Amorin, R., Balestra, I., Brusa, M., Calura, F., Castellano, M., Comastri, A., Fontana, A., Gilli, R., Mignoli, M., Pentericci, L., Vignali, C., & Zamorani, G. 2016, *ArXiv e-prints* 1602.00688
- Vanzella, E., Giavalisco, M., Dickinson, M., Cristiani, S., Nonino, M., Kuntschner, H., Popesso, P., Rosati, P., Renzini, A., Stern, D., Cesarsky, C., Ferguson, H. C., & Fosbury, R. A. E. 2009, *ApJ*, 695, 1163

TABLE 1
REST-FRAME OPTICAL LINE RATIOS

Object (1)	RA (J2000) (2)	Dec (J2000) (3)	z_{neb} (4)	M_* ($10^9 M_\odot$) (5)	$\text{SFR}_{\text{H}\alpha}$ ($M_\odot \text{ yr}^{-1}$) (6)	$F(\text{H}\alpha)$ ($\times 10^{-17}$) (7)	$\text{Log}([\text{N II}]/\text{H}\alpha)$ (8)	$\text{Log}([\text{O III}]/\text{H}\beta)$ (9)	$\text{H}\alpha/\text{H}\beta$ (10)	$[\text{O III}]/[\text{O II}]$ (11)	$12+\text{log}(\text{O}/\text{H})$ (O3N2) (12)
Q0100-BX239	01:03:13.709	13:15:16.128	2.3034	2.8	28.3	5.3 ± 0.2	< -1.11	$0.81^{+0.05}_{-0.05}$	4.76 ± 0.60	4.06 ± 0.39	< 8.12
Q0142-BX165	01:45:16.867	-09:46:03.468	2.3577	2.2	70.2	21.5 ± 0.3	$-1.53^{+0.17}_{-0.12}$	$0.80^{+0.01}_{-0.01}$	3.70 ± 0.09	3.88 ± 0.13	$7.98^{+0.04}_{-0.05}$
Q0207-BX74	02:09:43.154	-00:05:50.208	2.1889	5.2	58.1	16.7 ± 0.2	$-1.35^{+0.07}_{-0.06}$	$0.94^{+0.05}_{-0.04}$	4.13 ± 0.42	8.77 ± 0.34	$8.00^{+0.02}_{-0.03}$
Q0207-BX87	02:09:44.234	-00:04:13.512	2.1924	18.6	22.8	10.0 ± 0.2	< -1.16	$0.82^{+0.05}_{-0.05}$	3.41 ± 0.38	4.78 ± 0.33	< 8.10
Q0207-BX144	02:09:49.210	-00:05:31.668	2.1682	2.8	48.6	15.5 ± 0.2	< -1.44	$0.78^{+0.03}_{-0.03}$	3.98 ± 0.23	6.00 ± 0.21	< 8.02
Q0821-BX102	08:21:05.858	31:09:53.892	2.4151	6.3	27.0	12.3 ± 0.1	< -1.60	$0.82^{+0.01}_{-0.01}$	3.01 ± 0.08	8.99 ± 0.89	< 7.96
Q0821-BX221	08:21:06.898	31:08:08.160	2.3957	5.4	13.4	6.1 ± 0.2	< -1.21	$0.77^{+0.01}_{-0.01}$	3.03 ± 0.12	5.57 ± 0.53	< 8.10
Q1217-BX164	12:19:41.100	49:40:11.028	2.3310	2.2	83.3	5.7 ± 0.2	$-1.14^{+0.16}_{-0.11}$	$0.79^{+0.11}_{-0.09}$	7.38 ± 1.58	2.40 ± 0.17	$8.11^{+0.05}_{-0.06}$
Q1700-BX553	17:01:02.201	64:10:39.396	2.4719	2.8	21.8	8.3 ± 0.2	< -1.10	$0.75^{+0.03}_{-0.03}$	3.18 ± 0.22	7.16 ± 0.45	< 8.14
Q1700-BX711	17:01:21.288	64:12:20.664	2.2947	20.0	19.0	10.7 ± 0.2	$-1.25^{+0.10}_{-0.08}$	$0.80^{+0.02}_{-0.02}$	2.79 ± 0.12	4.89 ± 0.59	$8.08^{+0.03}_{-0.03}$
Q2206-BM64	22:08:52.354	-19:43:28.416	2.1943	8.5	27.4	7.8 ± 0.1	$-1.21^{+0.12}_{-0.12}$	$0.75^{+0.05}_{-0.05}$	4.15 ± 0.49	4.08 ± 0.26	$8.10^{+0.05}_{-0.06}$
Q2343-BX418	23:46:18.571	12:47:47.364	2.3054	2.8	52.0	14.0 ± 0.1	$-1.34^{+0.08}_{-0.07}$	$0.87^{+0.02}_{-0.02}$	4.02 ± 0.20	6.83 ± 0.31	$8.02^{+0.02}_{-0.03}$
Q2343-BX460	23:46:17.134	12:48:06.912	2.3945	1.9	14.1	5.8 ± 0.1	$-1.38^{+0.16}_{-0.11}$	$0.79^{+0.03}_{-0.02}$	3.19 ± 0.19	4.38 ± 0.30	$8.04^{+0.04}_{-0.05}$
Q2343-BX660	23:46:29.434	12:49:45.552	2.1742	5.4	28.8	18.5 ± 0.2	< -1.69	$0.79^{+0.02}_{-0.02}$	2.52 ± 0.13	12.15 ± 0.35	< 7.93

NOTE. — Column descriptions: (1) Galaxy ID (2–3) RA and Dec (J2000) (4) Systemic redshift from joint fit to the nebular emission lines. (5) Stellar mass in units of $10^9 M_\odot$, assuming a Chabrier (2003) initial mass function. (6) Star formation rate from extinction-corrected H α flux using the relationship of Kennicutt (1998). (7) H α flux in units of $10^{-17} \text{ erg s}^{-1} \text{ cm}^{-2}$. (8) Ratio of [N II] $\lambda 6584/\text{H}\alpha$. (9) Ratio of [O III] $\lambda 5007/\text{H}\beta$. (10) Observed H $\alpha/\text{H}\beta$ ratio with statistical errors; see text for discussion of additional systematic uncertainties due to slit loss corrections. (11) Observed ratio [O III] $\lambda\lambda 4959, 5007/[\text{O II}] \lambda\lambda 3727, 3729$, without correcting for extinction. (12) Oxygen abundance calculated with the O3N2 calibration of Pettini & Pagel (2004).

TABLE 2
Ly α PROPERTIES

Object	z_{neb}	$z_{\text{Ly}\alpha}$	$F(\text{Ly}\alpha)$ ($\times 10^{-17}$)	$W_{\text{Ly}\alpha}$ (\AA)	$\Delta v_{\text{Ly}\alpha}$ (km s^{-1})	Ly α /H α	$f_{\text{esc}}^{\text{Ly}\alpha}$
(1)	(2)	(3)	(4)	(5)	(6)	(7)	(8)
Q0100-BX239	2.3034	2.3067	5.3 ± 0.4	18.3 ± 2.0	296 ± 54	1.01 ± 0.09	0.04 ± 0.01
Q0142-BX165	2.3577	2.3590	28.2 ± 0.4	61.2 ± 2.3	114 ± 15	1.31 ± 0.03	0.09 ± 0.01
Q0207-BX74	2.1889	2.1882	27.3 ± 0.7	101.9 ± 4.4	-61 ± 36	1.64 ± 0.04	0.09 ± 0.02
Q0207-BX87	2.1924	2.1930	33.2 ± 0.7	77.3 ± 4.7	54 ± 21	3.33 ± 0.09	0.27 ± 0.07
Q0207-BX144	2.1682	2.1695	19.8 ± 0.9	37.5 ± 2.0	125 ± 61	1.28 ± 0.06	0.07 ± 0.01
Q0821-BX102	2.4151	...	< 0.78	< -3.25	...	< 0.06	< 0.007
Q0821-BX221	2.3957	2.3987	0.9 ± 0.3	7.7 ± 2.5	269 ± 212	0.15 ± 0.05	0.02 ± 0.01
Q1217-BX164	2.3310	2.3340	2.9 ± 0.1	22.0 ± 2.2	270 ± 19	0.51 ± 0.03	0.007 ± 0.003
Q1700-BX553	2.4719	2.4747	9.7 ± 0.5	33.7 ± 2.4	240 ± 43	1.16 ± 0.07	0.11 ± 0.02
Q1700-BX711	2.2947	2.2958	2.2 ± 0.5	20.4 ± 5.3	100 ± 212	0.21 ± 0.05	0.02 ± 0.01
Q2206-BM64	2.1943	2.1973	7.9 ± 1.0	22.9 ± 3.4	281 ± 85	1.02 ± 0.12	0.05 ± 0.02
Q2343-BX418	2.3054	2.3077	32.8 ± 1.2	61.8 ± 2.6	208 ± 57	2.34 ± 0.09	0.13 ± 0.02
Q2343-BX460	2.3945	2.3966	7.8 ± 0.4	47.7 ± 2.8	184 ± 71	1.35 ± 0.07	0.13 ± 0.02
Q2343-BX660	2.1742	2.1778	16.8 ± 0.7	40.4 ± 2.2	338 ± 43	0.91 ± 0.04	0.10 ± 0.02

NOTE. — Column descriptions: (1) Galaxy ID (2) Systemic redshift from joint fit to the nebular emission lines. (3) Ly α redshift from centroid of Ly α emission. (4) Ly α flux in units of $10^{-17} \text{ erg s}^{-1} \text{ cm}^{-2}$. (5) Rest frame Ly α equivalent width. (6) Velocity offset of the centroid of Ly α emission from the systemic redshift. (7) Observed Ly α /H α flux ratio. (8) Ly α escape fraction, assuming an intrinsic ratio Ly α /H α = 8.7 and with H α fluxes corrected for extinction based on the H α /H β ratio.